Highly polar states of Rydberg atoms in strong magnetic and weak electric fields

E. Paradis, S. Zigo,* and G. Raithel
Department of Physics, University of Michigan, Ann Arbor, Michigan 48109, USA
(Received 24 October 2012; published 14 January 2013)

We study the spectra of diamagnetic rubidium Rydberg atoms in strong magnetic and weak electric parallel fields, in the n-mixing regime. Our emphasis is on isolated pairs of near-degenerate, opposite-parity, diamagnetic states that become mixed by the weak electric field. Such level pairs allow for the generation of nondegenerate states with large, tunable permanent electric dipole moments and large optical excitation cross sections from the atomic ground state. We investigate how the dipole moments and the zero-electric-field energy defects of these level pairs can be tuned using small variations of the electric and magnetic fields. Using calculations, we explore the abundance of such level pairs over wide spectral regions for several magnetic quantum numbers. Applications of polar, diamagnetic Rydberg states in Rydberg-atom interaction experiments are briefly discussed.

DOI: 10.1103/PhysRevA.87.012505 PACS number(s): 32.30.−r, 32.80.Ee, 32.10.Dk, 32.10.Ee

I. INTRODUCTION

Control of coherent interactions between neutral atoms has shown considerable promise in quantum information processing. Recent experiments have demonstrated that Rydberg atoms, having long lifetimes and exhibiting long-range interactions, form a strong candidate system for creating quantum gates [1–3]. In particular, the effect of two types of long-range interactions, the dipole-dipole interaction [4–6] and the van der Waals interaction [7,8], have been investigated as possible coupling mechanisms. The Rydberg excitation blockade, which follows from these interactions, has been used to produce entangled pairs of atoms [9] and to implement a controlled-NOT (CNOT) gate [10].

In order to create a blockaded Rydberg system, both strong electrostatic Rydberg-Rydberg interactions as well as reasonably high optical excitation rates of the utilized Rydberg levels are necessary. One approach is to use states with large permanent electric dipole moments, which are found, for instance, in linear Stark states [11,12]. However, such states tend to have small optical excitation cross sections, and the close proximity of other Stark states can complicate the system through unwanted level crossings and state mixing. Another method is to utilize states that exhibit an energy exchange (Förster) resonance [6,13]. The energy defect of such resonances can be tuned to zero with either dc electric fields [4,14] or ac Stark shifts [15]. Under certain conditions, Förster resonances are ineffective because of the presence of Förster zeros [16], which are due to magnetic level degeneracies. Further, there are only a limited number of levels that exhibit Förster resonances within a given atomic species. Since robust atom-atom interaction schemes require insensitivity to moderate variations in experimental parameters (initial-state preparation, laser polarizations, stray electric and magnetic fields, etc.), level degeneracies and near-degeneracies should be avoided if at all possible. Degeneracy-free atomic levels enable more robust atom-atom interactions.

In this paper we explore the Rydberg-atom spectrum in the presence of both a strong magnetic field and a weak parallel electric field, with the aim of preparing states with large dipole moments, large optical excitation cross sections, and no close degeneracies with other states. The paper is organized as follows. In Sec. II, we discuss the properties of Rydberg atoms in parallel fields. This is followed by the experimental details in Sec. III, and presentation of observed spectra taken at fixed magnetic field and variable electric field in Sec. IV. In Sec. V, we investigate the effect of varying the magnetic field at fixed electric field. Then, in Sec. VI, we compare the measurements to numerical calculations, which offer additional insight into the abundance of states with the desired properties. We conclude with a discussion of the results in Sec. VII.

II. RYDBERG ATOMS IN PARALLEL ELECTRIC AND MAGNETIC FIELDS

The Hamiltonian for a Rydberg atom in parallel electric and magnetic fields can be written as

$$\hat{H} = \frac{\hat{p}^2}{2} - \frac{1}{\hat{r}} + F\hat{z} + \frac{B}{2}(\hat{\ell}_z + g\hat{s}_z) + \frac{B^2}{8}\hat{\rho}^2 + \hat{V}_{LS} + \hat{V}_C(r). \tag{1}$$

Here, the electric and magnetic fields F and B are directed along the z axis, $\hat{V}_{LS}$ represents the fine structure, and $\hat{V}_C$ is the core potential, which can be accounted for through the quantum defects [11,12]. The operators $\hat{\ell}_z$ and $\hat{s}_z$ represent the orbital and spin angular momenta of the Rydberg electron in the field direction, and $g \approx 2.002\,31$ is the electron g factor. Because of azimuthal symmetry, the total angular momentum $\hat{j}_z = \hat{\ell}_z + \hat{s}_z$ is conserved. The diamagnetic term, $\frac{B^2}{8}\hat{\rho}^2$ (where $\hat{\rho}^2 = \hat{x}^2 + \hat{y}^2$), becomes important in the case of a strong magnetic field. When $F = 0$ there exists another important symmetry, namely the parity Π_z along the z axis [12]. The parity Π_z is a discrete symmetry (even or odd). We are interested in the case of strong magnetic and relatively weak electric fields.

As the magnetic field is increased, the system progresses through several qualitatively different regimes. In the case of low magnetic fields, where the diamagnetic term is vanishing ($B \ll 2n^{-4}$ in atomic units), the linear Zeeman shift lifts some of the zero-field Rydberg level degeneracies by separating

*Present address: Department of Physics, Kansas State University, Manhattan, KS 66506.

states of different magnetic quantum numbers m_J. However, quantum-defect-free states of the same m_J and n are still approximately degenerate. If the magnetic field is further increased, the diamagnetic component of the Hamiltonian becomes important, lifting most of the remaining degeneracies. The energy spectrum in the ℓ-mixing regime ($2n^{-4} \lesssim B \lesssim 2n^{-3.5}$) is organized in rotator and vibrator states [17,18]. Rotator states are nondegenerate and have wave functions extending mostly in the plane transverse to B. They have large diamagnetic shifts and large magnetic dipole moments. Vibrator states have wave functions extending mostly in the direction of B. Their diamagnetic shifts and magnetic dipole moments are relatively small. They are twofold degenerate, with one state having even Π_z and the other having odd Π_z. As B is further increased, the system reaches the n-mixing regime ($B \gtrsim 2n^{-3.5}$) [19,20]. Here, the level structure organization in rotator and vibrator states, and the vibrator-state degeneracies, are increasingly lost, and Rydberg levels become more or less evenly spread out in energy. Due to the latter aspect, (near-)degeneracies become less likely, although some near-degenerate vibrator pairs still exist up to comparatively high magnetic field strength. Above the n-mixing regime, for $B \gtrsim 2n^{-3}$ the system becomes classically chaotic and exhibits signatures of "quantum chaos" [11].

The regime of interest in this paper is the n-mixing regime, where the levels are well spread out and a few near-degenerate vibrator pairs are left. At $B \approx 2.6$ T, this corresponds to a range of $32 \lesssim n \lesssim 56$ (or equivalently -108 to -35 cm^{-1}). The calculations presented throughout the paper are accurate over that entire range. At energies above -35 cm^{-1}, the density of states generally becomes so high that *isolated*, near-degenerate level pairs with the mixing properties described in the following paragraph and with negligible perturbation from nearby states cease to exist. Most of our studies are at scaled energy $\varepsilon = EB^{-2/3} \approx -0.5$ in atomic units (the scaled energy is discussed in Ref. [11], section 5.3.5, and references therein), with $B \approx 2.6$ T and $E \sim -55$ cm^{-1}. In this regime, the instantaneous magnetic dipole moment, given by the level energy slope $(-\partial E/\partial B)$, varies widely from state to state. The magnetic moments of remnant, near-degenerate vibrator pairs tend to be relatively low and somewhat different from each other, due to varying, small admixtures of states extending in the plane transverse to B (see the wave-function examples discussed in Sec. VI). These admixtures are so small that they do not fundamentally alter the character of the states, but they are sufficient to cause small variations in the magnetic dipole moments of the states. The resultant differential response of near-degenerate vibrator pairs to magnetic field changes can be used to tune the pairs into resonance (discussed in more detail in Sec. V).

If a small electric field F parallel to B is applied, nondegenerate states exhibit small quadratic Stark shifts in F. However, near-degenerate pairs of vibrator states of the same m_J and opposite Π_z become mixed and lose their well-defined Π_z character already at low values of F. If the two near-degenerate states are vibrator states of similar overall wave-function structure and opposite Π_z, the F-induced mixing induces large, opposite electric dipole moments in the state pair, which result in large linear Stark shifts. The behavior of such electric-field-coupled pairs of vibrator states is akin to state pairs in a symmetric one-dimensional double-well potential,

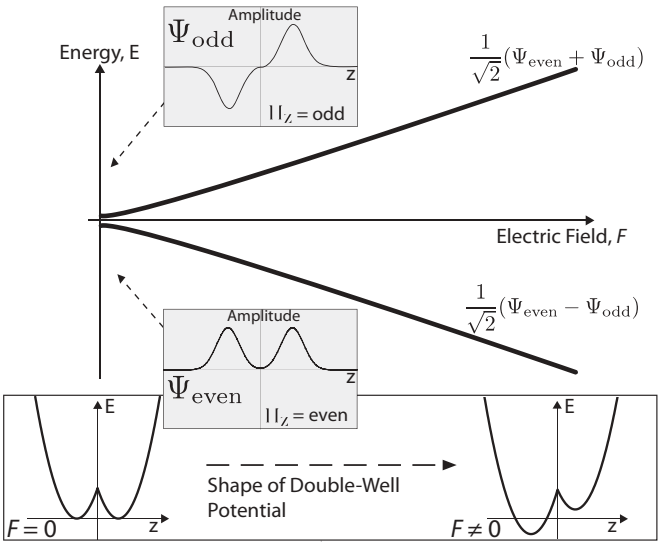

FIG. 1. Electron in a one-dimensional, symmetric double-well potential perturbed by an electric field F. For $F = 0$ the double-well system has discrete Π_z symmetry, which is lost when $F \neq 0$. As explained in the text, this simple model system mimics the essential properties of electric-field-coupled vibrator states of Rydberg atoms in strong magnetic and weak parallel electric fields.

as illustrated in Fig. 1. Considering identical harmonic wells connected at $z = 0$, the oscillation frequency ω_{osc} and its inverse, the density of states, are set by the particle mass and the force constant in the individual wells. The separation of the wells determines how many sub-barrier levels each well holds. As sketched in Fig. 1, the sub-barrier states are grouped in near-degenerate pairs, with one state being an even and the other an odd superposition of the single-well states. The tunneling-induced energy differences of the pairs can be estimated by the Gamow factor times ω_{osc}. The effect of an electric field F is equivalent to a relative energy shift between the wells, which lifts the near-degeneracy of the sub-barrier-state pairs. When the energy shift exceeds the tunneling frequency, the state energies become linear in F and the eigenstates become localized in the individual wells (corresponding to 50:50 superpositions of the even- and odd-parity states). These characteristics are summarized in Fig. 1. For particles of one electron mass and elementary charge, $\omega_{osc} \sim 10$ GHz, and well minima at $\pm 2000 a_0$, the level spectra mimic those in our experiment. For these parameters, about three sub-barrier levels fit within each well. The ground-state level pair has a tunneling-induced splitting of $\sim$10 MHz, and in an electric field F the dipole moments are $\pm 2000 e a_0$. The double-well model, sketched in Fig. 1, can provide guidance in our high-magnetic-field system when near-resonant vibrator states of opposite parity become mixed by an applied electric field.

III. EXPERIMENTAL METHOD

In the experiment, cold Rydberg atoms are excited via a stepwise narrowband photoexcitation process in a 2.6 T high-field atom trap. Several tens of millions of ^{85}Rb atoms are laser cooled to the Doppler limit ($\sim$150 μK) and magnetically confined within the Ioffe-Pritchard trap. The trapped atom

cloud is cigar shaped of axial full width at half maximum (FWHM) of 4.0 mm and transverse FWHM of 2.2 mm. The size of the trap is an invariable parameter of the superconducting-coil geometry in the available high-field atom trap. The trap size is not well matched to the size of the excitation region, discussed in the following paragraph. The atom density in the trap is $\sim 10^9$ cm^{-3}. We have experimentally determined that this density is too low for Rydberg excitation blockade effects [4] to play a role for the excitation energy range of interest in this paper. For a detailed description of the high-magnetic-field trapping apparatus see Refs. [21,22]. The magnetic field is stable to <1 G and can be varied in discrete steps of 10 G. Rydberg atoms are produced via two-photon excitation at 780 and 480 nm (laser linewidths $\leqslant 1$ MHz) through the intermediate $5P_{3/2}|m_I = 5/2, m_J = 3/2\rangle$ state. We are able to excite and detect states with energies ranging from ~ -90 cm^{-1} up into the ionization continuum; this experimentally accessible range overlaps well with the above-mentioned range of interest (-108 to -35 cm^{-1}).

The excitation pulses are of variable duration (10–100 μs) and are focused into the trap with respective FWHMs of the intensity profiles of 60 and 20 μm, respectively. The excitation beams are crossed at the trap center, resulting in a small excitation region and ensuring that the Rydberg states are produced in a well-defined, uniform magnetic field. While the magnetic field varies by about 1 G over the entire trapping region, the variation within the Rydberg excitation region is only in the tens of milligauss range. The intensity of the lower (780 nm) excitation pulse is set to $\sim 5 I_{\rm sat}$ ($I_{\rm sat} = 1.6$ mW/cm^2) as a compromise between count rate and power broadening, while the upper (480 nm) pulse has a total power of 20 mW for an intensity maximum of 2×10^6 mW/cm^2 at the focus. Excitation of the strongest lines is heavily saturated for these intensities. At the current trap density and Rydberg excitation energy, no Rydberg blockading effects occur. The observed Rydberg excitation lines have FWHM linewidths ~ 10 MHz, as measured by scanning the upper-transition laser frequency and reading out the generated Rydberg-atom population as explained in the following paragraph. These linewidths are limited by the power broadening of the $5S \rightarrow 5P$ transition; there is no measurable power broadening due to the upper excitation stage. Since we employ laser-cooled atoms, there is no line broadening due to residual Doppler shifts and Lorentz electric fields ($\mathbf{F}_{\rm Lorentz} = \mathbf{v} \times \mathbf{B}$). Also, the ground-state atom sample is spin polarized.

The electric field F is parallel to B and is applied during the excitation pulse by varying the relative potential between two electrodes surrounding the trap. The value of F can be controlled to within an accuracy of 0.2 V/m, limited by 60 Hz noise on the electrodes. Immediately following the excitation, a much stronger field ionization ramp of short duration (5 μs) is applied to the electrodes. The resulting field-ionized electrons are directed toward a microchannel plate (MCP) detector assembly located outside of the high-field region. The MCP has a detection efficiency of $\lesssim 50\%$ (from the manufacturer technical note [23]). The detector assembly provides both countable pulses as well as blips on a phosphor screen, allowing for both temporal and spatial count resolution.

Only ground-state atoms with $m_J = m_{\rm s} = +1/2$ are low-field-seeking and are contained within the atom trap. Since we excite Rydberg atoms with a stepwise two-photon process via the intermediate $5P_{3/2}|m_I = 5/2, m_J = 3/2\rangle$ state, there are only three optically accessible manifolds of Rydberg levels, namely, $m_J = 1/2$, $3/2$, and $5/2$. The accessible manifolds, which we write as $m_J = \{1/2, 3/2, 5/2\}$, are not coupled by parallel B and F fields pointing in the z direction. Although the time-independent states are of constant m_J and can be expressed as linear combinations of basis states with well-defined m_ℓ and $m_{\rm s}$, the strong magnetic field decouples the fine structure, and almost all time-independent states have expectation values of either $\langle \hat{s}_z/\hbar \rangle \approx 1/2$ or $\langle \hat{s}_z/\hbar \rangle \approx -1/2$. Since only the states with $\langle \hat{s}_z/\hbar \rangle \approx 1/2$ are accessible via optical excitation from our intermediate $5P$ level, only about half of the time-independent states in the manifolds $m_J = \{1/2, 3/2, 5/2\}$ are experimentally excitable, with respective expectation values $\langle \hat{\ell}_z/\hbar \rangle \approx \{0, 1, 2\}$. In addition, for $F = 0$ the Rydberg levels have well-defined parity Π_z. Since the intermediate $5P_{3/2}|m_I = 5/2, m_J = 3/2\rangle$ state is $\Pi_z =$ even, at $F = 0$ parity conservation considerations yield $\Pi_z = \{\text{even}, \text{odd}, \text{even}\}$ for the optically accessible Rydberg states with $m_J = \{1/2, 3/2, 5/2\}$, respectively. Hence, when parity and spin-selection considerations are combined, at $F = 0$ only about one-quarter of the time-independent states within the manifolds $m_J = \{1/2, 3/2, 5/2\}$ have substantial excitation rates.

IV. LEVEL STRUCTURE AT FIXED MAGNETIC AND VARIED ELECTRIC FIELDS

We first consider spectra taken at fixed magnetic field B of approximately 2.58 T, and F ranging from zero to about 50 V/m. Figure 2(a) shows the Rydberg states observed as a function of frequency as the upper-transition (480 nm) laser is

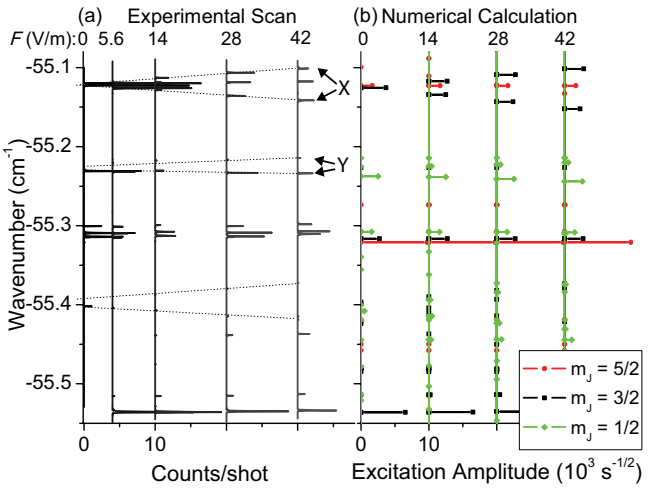

FIG. 2. (Color online) (a) Rydberg levels observed in the vicinity of scaled energy $\varepsilon \approx -0.51$, probed by scanning the upper-transition laser frequency, for $B_{\rm expt} = 2.577$ T, and at the indicated electric field values. Level energies are shown with respect to the field-free photoionization threshold. Some close-lying level pairs of the same m_J exhibit large and opposite electric dipole moments (slopes of the dotted lines). (b) Calculated line spectra, as detailed in Sec. VI, for $B_{\rm th} = 2.581$ T. In the calculations states of both parities are shown for all optically accessible m_J levels. Hence, numerous calculated levels are experimentally undetectable.

scanned over several gigahertz at a scaled energy $\epsilon \approx -0.51$, with excitation pulses of 100 μs duration. The polarization of the 480 nm laser is set mostly parallel to the B field axis to excite $m_J = 3/2$ states. Due to the beam's angle of incidence, a small amount of the orthogonal polarization is also present, so that $m_J = 1/2$ and $5/2$ states are also excited. Additional scans, similar to those shown in Fig. 2(a), have been taken in several higher-lying energy ranges. Since all scans recorded are in the n-mixing regime, the observed Rydberg states are fairly evenly spread out and, with a few exceptions, nondegenerate.

For the spectra to be suitable for studies involving coherent Rydberg-atom interactions, the average density of states should be lower than the inverse of anticipated Rydberg-atom interaction energies, so that off-resonant levels can be ignored. Since anticipated Rydberg-atom interaction energies are on the order of tens of megahertz (see Sec. VII), densities of states well below ~100/GHz are desired. From Fig. 2(a) and similar data, for $F = 0$ we determine average densities of states of 0.5/GHz and 1.9/GHz at energies of -55 and -19 cm^{-1}, respectively. The average density of states increases with excitation energy, but it is always well below ~100/GHz over the mentioned energy range. Therefore, we expect to find quantum states that are far away from other levels and that are conducive to strong atom-atom interactions (by having large electric dipole moments, for instance).

The experimentally observed densities of states compare well with a semiclassical calculation of the average densities of states using the Weyl theorem (see Eq. 16.4 in Ref. [24]). Counting only states of one Π_z parity, the semiclassical calculation yields state densities of 0.57/GHz and 1.6/GHz for -55 cm^{-1} and -20 cm^{-1}, respectively. These results are sums over the three optically accessible manifolds. The local density of states varies about the given average values in a manner that can be revealed only by measurements or calculations of the actual quantum spectrum described by Eq. (1). The level statistics and the level distribution depend on how deep the system is in the "quantum-chaotic" regime, where level repulsion occurs. For detailed discussions of this topic, see Refs. [11,24], and references therein.

While the above average densities of states are fairly low, near-degeneracies of states of the same m_J do occur. From the viewpoint of creating states with large electric dipole moments, the most interesting candidates are degeneracies between states of same m_J and opposite parity, which we may refer to as $|1\rangle$ and $|2\rangle$. In that case, a weak parallel electric field F can be used to generate states with a permanent electric dipole moment $p_0 = -e\langle 1|z|2\rangle$, and large linear Stark shifts. The detailed behavior depends on the overlap between $|1\rangle$ and $|2\rangle$, and on the energy defect at $F = 0$. We explore the behavior in Fig. 2(a). Some energy levels shift strongly as a function of F, while others are largely unaffected. For instance, the level pair labeled "X" in Fig. 2 exhibits strong linear Stark shifts. The level pair X represents a near-degenerate pair of vibrator states of opposite parity, as discussed in Sec. II. To reveal more detail near $F = 0$, in Fig. 3 we show a set of higher-resolution scans of the same pair over a much smaller range of F. From Fig. 3 the permanent dipole moment of the X pair of levels, given by the negative slope, is found to be $\pm 1500\, ea_0$. The magnitude of the permanent electric dipole moment of the X pair is quite large; it is about half the dipole moment of

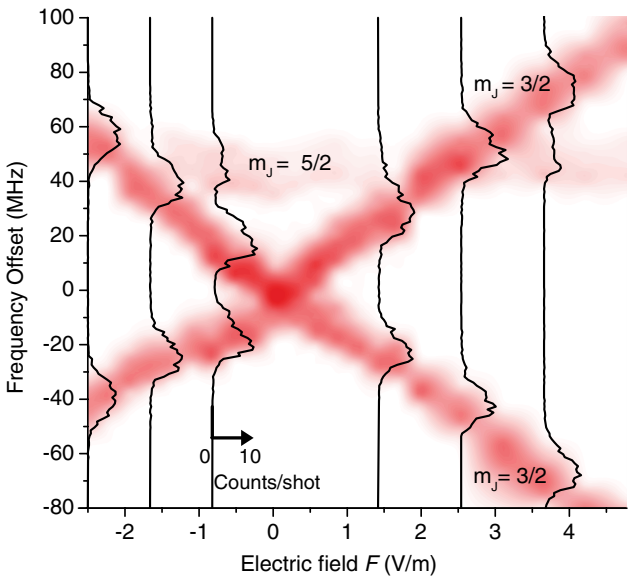

FIG. 3. (Color online) High-resolution contour plot showing the pair of Rydberg states labeled X in Fig. 2 at -55.1 cm^{-1}, with $B_{\text{expt}} = 2.576$ T and excitation pulse lengths of 10 μs. Excitation frequency versus applied electric field (V/m) is plotted, with color representing the observed excitation rate (white 0, red 14 counts per shot). The electric field is varied in steps of 0.3 V/m, and a few selected scans are overlaid as black lines. The weak state at a fixed frequency offset of about 40 MHz has $m_J = 5/2$, and is excited due to imperfect polarization. The $m_J = 5/2$ state has a negligible Stark shift and does not couple to the $m_J = 3/2$ pair of states.

extreme Stark states of Rydberg atoms in no magnetic and weak electric fields [which is $(3/2)n^2 = -3/(4E)$ in atomic units [25]]. The X pair of levels becomes degenerate at a local electric field of $F = 0$ V/m, as shown in Fig. 3. We note that in the experiment the degeneracy is observed at an applied voltage of 16 mV, corresponding to an offset field of $F = 0.9$ V/m. The small offset is likely due to static patch or contact potentials, or caused by the analog control electronics.

The X pair of states in Figs. 2 and 3 are 50:50 mixtures of a Π_z-even and a Π_z-odd state at all values of F. Since in the experiment we excite one definite parity (odd parity for $m_J = 3/2$), both components of the pair should exhibit equal line strength, regardless of F. Figures 2 and 3 show that for the X pair of states this is indeed the case. It is noted that an exact crossing, as shown in Fig. 3, requires a well-tuned magnetic field. The resonant magnetic field value is different for each individual set of near-degenerate states (see Sec. V). The case of coupled vibrator states that are near-degenerate at $F = 0$ is visualized by the model in Fig. 1, where the double well is assumed to be symmetric.

In our regime of study, most electric-field-coupled pairs of vibrator states encountered are nondegenerate at $F = 0$, with an energy defect on the order of $\Delta E \sim 100$ MHz. An instance of that case, which would correspond to an asymmetric double-well potential in Fig. 1, is found in the Y pair of lines in Fig. 2(a). In that case, the time-independent states maintain opposite parities Π_z at small values of F. It takes a substantial field F for the Stark shifts to become comparable to the energy

defect ΔE, and for substantial state mixing to occur. Since in our experiment only one parity is optically excited, one observes highly asymmetric line strengths up to values of F at which the Stark shifts become larger the energy defect ΔE. If F is increased further, the line-strength ratio of such state pairs trends toward unity. Those characteristics are found in the Y pair of lines in Fig. 2(a).

V. MAGNETIC FIELD TUNING OF NEAR-DEGENERATE STATES

The magnetic field dependence of Rydberg level energies can be used to tune near-degenerate opposite-parity vibrators states into resonance, i.e., to tune their energy defect ΔE. This enables the creation of highly polar states by application of a weak parallel electric field F. As an example, in this section we show that the X pair of levels in Figs. 2 and 3 can be tuned through resonance at $F = 0$ by exploiting the difference in their magnetic moments.

Since the diamagnetic shift depends on the transverse spread of the wave function, which varies from state to state, usually one can use the magnetic field to fine-tune the energy defect ΔE of any arbitrary level pair. Lines observed near $-55\ \mathrm{cm}^{-1}$ and $B \approx 2.6$ T bear a range of instantaneous magnetic dipole moments varying from 0 to $-20\mu_B$. We measure the magnetic dipole moments by incrementing the magnetic field by a small amount $\Delta B = 10$ G, corresponding to a 0.04 % change of the 2.6 T field, and then measuring the corresponding energy shifts of the Rydberg states of interest. In Fig. 4(a) we show the response of the level pair marked X in Fig. 2. A slight electric field, $F \approx 1$ V/m, is applied to resolve the two states in the crossing region. It is noted that in Fig. 4(a) all three energy levels exhibit a large common shift as a function of magnetic field, indicating that all three states

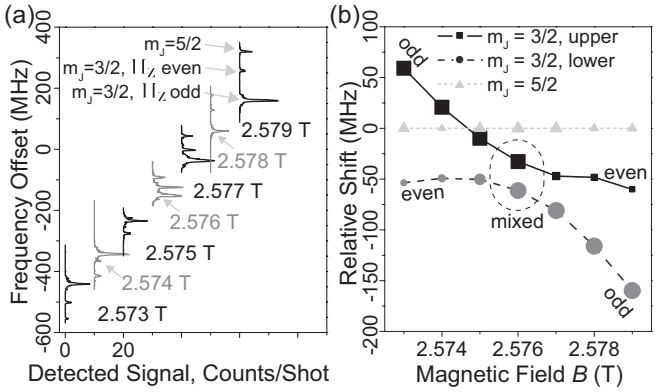

FIG. 4. (a) Scans of the state pair labeled X in Fig. 2 for the indicated magnetic field values and a weak parallel electric field $F \approx 1$ V/m. We show the line shifts relative to that of the $5P_{3/2}|m_J = 5/2, m_J = 3/2\rangle$ level. The two states of opposite parity have different magnetic dipole moments, of $-9.2\mu_B$ ($-11.7\mu_B$) for the odd- (even-) parity peak. (b) Levels of the X pair of states, which both have $m_J = 3/2$, relative to the $m_J = 5/2$ level, which is used as a convenient reference line. The symbol size qualitatively represents the line strength. The X pair of states exhibits an anticrossing (instead of an exact crossing) because of the coupling induced by the weak electric field F.

have similar magnetic dipole moments. In identifying which Rydberg levels correspond to each other in the displayed scans, it helps to note that the three levels fall on three approximately straight lines, indicating that the individual magnetic dipole moments of the three levels are fairly constant throughout the displayed magnetic field range (values provided in the caption of Fig. 4). This is clearly seen in Fig. 4(b), where we show the measured frequency shifts of the two $m_J = 3/2$ levels relative to a convenient $m_J = 5/2$ reference line (which does not couple to $m_J = 3/2$ levels). The observed line strengths of the states are visualized by the size of the plotted symbols. Away from the crossing region the applied electric field is insufficient to couple the states. There, only the odd state is observed while the even one is (almost) undetectable, and both states have zero electric dipole moment. At resonance ($B = 2.576$ T), the weak electric field couples the even- and odd-parity levels into highly polar states that have equal optical excitation cross sections.

The width of the anticrossing, measured to be 28 MHz in Fig. 4(b), is in good qualitative agreement with a simple two-state Hamiltonian:

$$\hat{H}_2 = -\mu_1(B - B_0)|1\rangle\langle 1| - \mu_2(B - B_0)|2\rangle\langle 2| + Fp_0(|1\rangle\langle 2| + |2\rangle\langle 1|). \quad (2)$$

Here, μ_1 and μ_2 are the magnetic dipole moments of states $|1\rangle$ and $|2\rangle$, respectively. For the magnetic dipole moments given in Fig. 4, an electric dipole moment of $p_0 = 1500\, ea_0$ (derived from Fig. 3), and with $F = 1$ V/m, the level separation at the resonant magnetic field ($B = B_0$) is $2Fp_0 = h \times 38$ MHz. This is in good qualitative agreement with the measured value of 28 MHz. The discrepancy is due to the experimental level resolution (10 MHz), the electric field uncertainty (0.2 V/m, i.e., 20% of the field applied in Fig. 4), and the uncertainty of the measured electric dipole moment ($\sim 100\, ea_0$). We are able to reduce the applied electric field F such that the two $m_J = 3/2$ states in Fig. 4 exactly cross to within the experimental level resolution of 10 MHz.

In this section we have shown that magnetic field control allows one to shift pairs of remaining vibrator-state pairs of the same m_J but opposite Π_z into resonance with one another. These resonant states can then be subjected to a parallel electric field F in order to form highly polar nondegenerate states with large electric dipole moments that are fairly insensitive to F. Choosing an electric field F of a few 10 V/m separates the polar states by several 100 MHz. This setting will be ideal for Rydberg-atom interaction schemes that require atoms in well-defined, nondegenerate, and highly polar states.

VI. LEVEL AND WAVE-FUNCTION CALCULATIONS

We have complemented our experimental results with numerical calculations of Rydberg spectra and wave functions in parallel electric and magnetic fields. The electric dipole and the diamagnetic matrix elements required for the diagonalization of the Hamiltonian in Eq. (1) are computed with numerically obtained Rydberg electron wave functions. For the fine structure parameters and the quantum defects we use previously published values [12,26]. For each m_J, we use a spherical basis set that includes all states with principal quantum numbers between 10 and 90. The value of m_J is

fixed for any given diagonalization. The Hamiltonian matrix is numerically diagonalized for given field value parameters B and F using LAPACK routines. Energy levels and excitation amplitudes from the intermediate $5P_{3/2}|m_I = 5/2, m_J = 3/2\rangle$ state are calculated for the optically accessible manifolds $m_J = \{1/2, 3/2, 5/2\}$. Figure 2(b) shows the resulting calculated spectrum and transition amplitudes over the same spectral region that was used in the experiment [Fig. 2(a)]. There, we have defined the transition amplitude into a Rydberg state $|\psi\rangle$ as the square root of the nonsaturated excitation rate $4\Omega_R^2/\Gamma$. Here, Ω_R is the Rabi frequency $\Omega_R = -eF_0\hat{\boldsymbol{\epsilon}} \cdot \langle\psi|\hat{\mathbf{r}}|5P_{3/2}, m_J = 3/2\rangle/\hbar$ in rad/s. The parameter Γ is the effective bandwidth of the optical excitation in rad/s. The laser field amplitude is denoted as F_0, the electric dipole operator $-e\hat{\mathbf{r}}$, and the polarization unit vector $\hat{\epsilon}$. For the manifolds $m_J = \{1/2, 3/2, 5/2\}$, the polarization unit vectors in the calculation are set to $\hat{\epsilon} = \{\hat{x}, \hat{z}, \hat{x}\}$, respectively. The effective level width is set to $\Gamma = 2\pi \times 10$ MHz, according to typical experimentally observed linewidths. The laser electric field F_0 is set in accordance with an intensity of $I = 2 \times 10^6$ mW/cm^2, as used in the experiment. Comparing Figs. 2(a) and 2(b) we find good agreement between calculated and experimental results, in terms of both absolute frequency and relative line strengths. Further, comparing calculations with varying basis sizes we find our simulated spectra to be useful up to energies of about -20 cm^{-1}.

The best agreement between experimental and simulated spectra is obtained when the simulated magnetic fields are taken to be 0.005 T higher than the ones used in the experiment, corresponding to a discrepancy of 0.2%. This magnetic field offset is consistent from day to day. We believe that the offset is due either to a calibration error in the magnet system, or to a minor variation of the main trap magnet over about ten years of use.

We have used the calculations in order to obtain the distribution of electric and magnetic dipole moments of Rydberg levels in selected spectral regions. These moments are important for applications that involve Rydberg-atom interactions. We calculate the instantaneous magnetic dipole moments by slightly incrementing the magnetic field at $F = 0$. The results can be used to predict the magnetic trapping behavior of the Rydberg levels. As shown in the histograms in Fig. 5(a), in the interval from -60 to -50 cm^{-1} (all within the n-mixing regime, representing the region about the experimentally observed lines at ~ -55 cm^{-1}) the probability distributions of the magnetic moment exhibit fairly well-defined bell-shaped maxima. The magnetic dipole moments are quite large, with means $\{-10.8\mu_B, -12.1\mu_B, -13.3\mu_B\}$ for the respective optically accessible manifolds $m_J = \{1/2, 3/2, 5/2\}$. The standard deviations are $\{4.0\mu_B, 4.8\mu_B, 5.5\mu_B\}$. The extreme values are $0\mu_B$ and $-27\mu_B$.

Knowledge of the electric dipole moments is important, for instance, to estimate the permanent electric dipole interaction between Rydberg-atom pairs. We determine the permanent electric dipole moments by performing two calculations with parallel electric fields $F = 3$ and 3.3 V/m, and calculating the energy shift of each state. As shown in Fig. 5(b), the distributions of magnitudes of the electric dipole moments are peaked at values below $100\,ea_0$, while typical averages are $400\,ea_0$ and standard deviations $800\,ea_0$. The distributions of

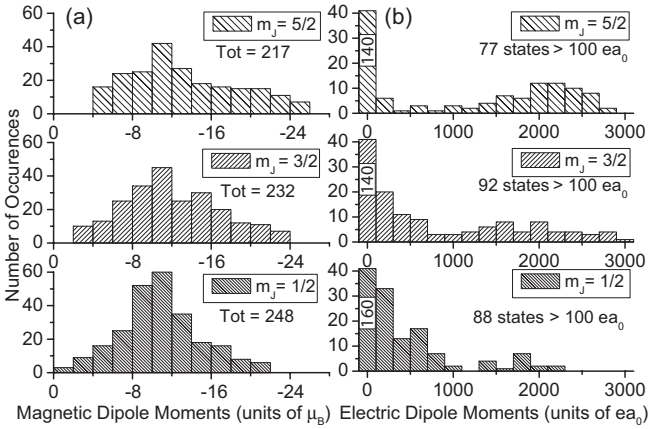

FIG. 5. (a) Histograms of all magnetic dipole moments in the interval from -60 to -50 cm^{-1}, for $B_{\text{th}} = 2.581$ T. For each value of m_J, the total number of Rydberg states in this interval is indicated below the legend. (b) Histograms of all electric dipole moment magnitudes, for the same energy interval and magnetic field value, with an applied electric field of $F = 3$ V/m. For clarity, the bars with dipole moments $<100\,ea_0$ are cut off at height 40, with the number of occurrences indicated on the bar.

the electric dipole magnitudes tend to have bimodal shapes, with a dominant first group of states close to zero and a second group with electric dipole moments up to a few thousand ea_0. Most energy levels in the n-mixing regime are clearly nondegenerate, resulting in small electric polarizabilities and small electric dipole moments at low values of F. This majority of levels gives rise to the first group in the electric-dipole distributions. The second group is due to remnant pairs of near-degenerate vibrator states of opposite parity and similar overall shape, such as the state pair X analyzed in Figs. 2 through 4. While the second group of states is much smaller than the first, it drives up the magnitudes of the averages and standard deviations.

The abundance of state pairs with large and approximately opposite electric dipole moments, such as the X and Y pairs in Fig. 2, is of primary interest for applications that involve electric dipole Rydberg-atom interactions. We determine the number of such pairs by parsing the computed spectra for pairs of neighboring lines with the same m_J and large, opposite electric dipole moments of similar magnitude (to within 30%). In the considered energy range -60 to -50 cm^{-1}, the manifolds $m_J = \{1/2, 3/2, 5/2\}$ include a total of 697 levels. The numbers of pairs with electric dipole moments greater than $100\,ea_0$ and with excitation amplitudes larger than 0.3×10^3 s$^{-1/2}$ are $\{14, 17, 10\}$. In Fig. 6 we show the distribution of these pairs versus dipole moment and excitation amplitude. We observe a weak trend that excitation amplitude diminishes with dipole moment. However, even for the highest dipole moments, which are of order $2000\,ea_0$, one can still find state pairs with fairly large excitation amplitudes (states within the dotted region in Fig. 6).

We have used the calculations to test our detailed experimental analysis of the X pair of states. Using a procedure equivalent to the one used in Fig. 4, by varying the magnetic field we obtain the resonant magnetic field value at which the level pair is degenerate. We find a theoretical resonant

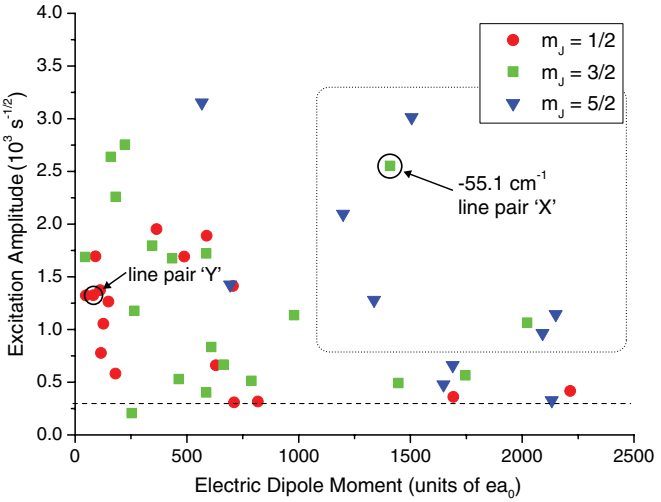

FIG. 6. (Color online) Scatter plot of line pairs with electric dipole moments $>100\,ea_0$ at $B_{\rm th} = 2.581$ T and $F = 3$ V/m, for the energy range between -60 and -50 cm^{-1}. The pairs are plotted versus dipole moment and excitation amplitude. The dashed line indicates our experimental excitation-amplitude limit above which lines can be easily observed.

magnetic field value of $B_{\rm th} = 2.581$ T. As mentioned above, this value differs by 0.005 T from the experimentally observed one ($B_{\rm expt} = 2.576$ T). The calculated magnetic dipole moments of the Π_z-odd and Π_z-even states of the X pair are $-9.4\mu_B$ and $-11.6\mu_B$, respectively. These values agree well with the measured values of $-9.2\mu_B$ and $-11.7\mu_B$ from Fig. 4. Further, the calculations yield an average electric dipole moment of $1410\,ea_0$ for the X pair. This value compares well to the measured value of $1500\,ea_0$. The 7% discrepancy probably arises from the uncertainty of the exact position of the excitation region within the inhomogeneous applied electric field. Also, in the experiment the electric field might have a very small component transverse to the magnetic field, which is not included in the calculations.

In order to further explore the nature of the state pairs with large electric dipole moments, we have calculated Rydberg-state wave functions. In Fig. 7, we plot the wave-function probabilities for the X pair of states at $B_{\rm th} = 2.589$ T and $F = 0$. The wave-function structures reiterate that the X pair represents an instance of a remnant pair of vibrator states in the n-mixing regime. The two wave functions differ slightly in the exact amount of admixtures of states that extend in the xy plane (the region near $z = 0$ and $\rho \gtrsim 2000a_0$). This gives rise to the difference in magnetic dipole moments, which we have employed to tune the level pair into resonance at $F = 0$ (see Sec. V). The large size of the electric dipole moments that result from the F-induced coupling between these two states stems from the fact that their wave functions have similar extents and node line patterns. The probability distributions of the wave functions of the coupled states under an applied electric field of $F = 3$ V/m are shown in Fig. 8. The coupled states are even and odd linear superpositions of the wave functions at $F = 0$; it is clear from Fig. 8 that the coupled states have large and opposite permanent electric dipole moments.

To conclude our theoretical considerations, we have performed classical trajectory calculations that demonstrate the

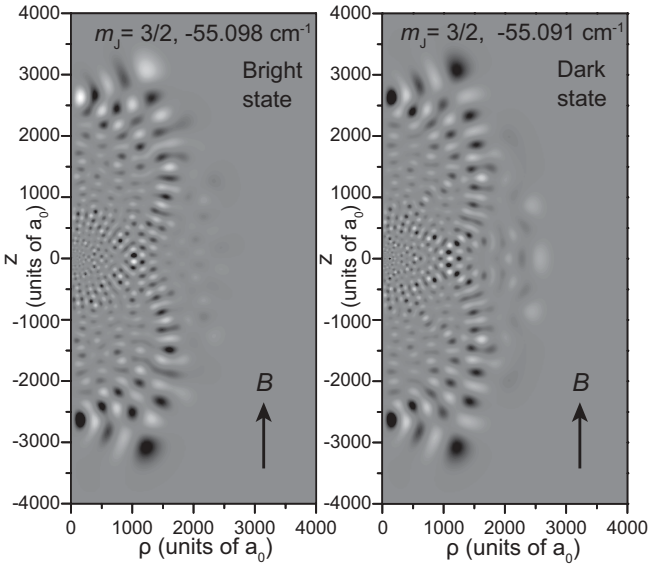

FIG. 7. Calculated normalized electron wavefunction probabilities $P = |\psi(\mathbf{r})|^2 r \sin\theta$ for the X line pair at -55.1 cm^{-1} with $B_{\rm th} = 2.589$ T and $F = 0$ V/m, on a grayscale gradation. Midlevel gray represents zero probability, while both white and black correspond to maximum probability. Dark (light) lobes in the probability distributions correspond to a negative (positive) wavefunction sign, to show whether Π_z is even or odd.

vibrator character of the X pair of levels. The trajectory calculations also show that the X pair and other remnant vibrator states in the n-mixing regime are associated with a classically regular domain of phase space, where classical and quantum dynamics exhibit close correspondence. In Fig. 9(a) we display two trajectories of a classical Rydberg electron at $B = 2.580$ T, energy -55.1 cm^{-1}, and electric field $F \approx 0$.

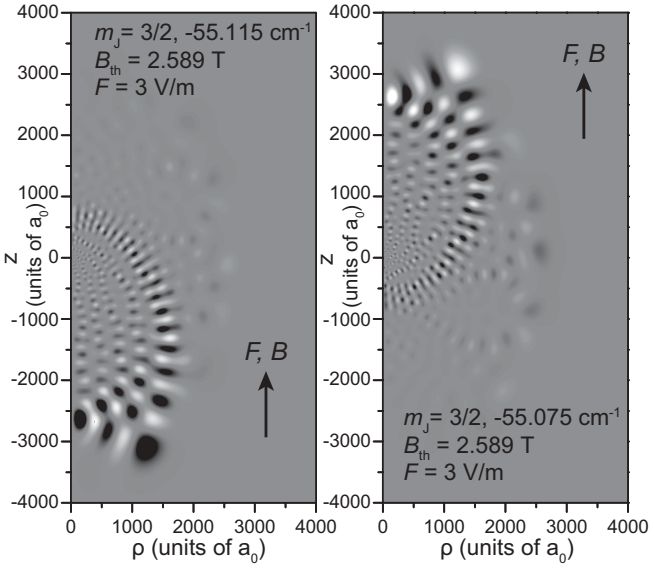

FIG. 8. Calculated normalized electron wavefunction probabilities $P = |\psi(\mathbf{r})|^2 r \sin\theta$ for the X line pair at ~ -55.1 cm^{-1} with $B_{\rm th} = 2.589$ T, with a weak parallel electric field of $F = 3$ V/m. The F-induced coupling leads to the displayed states with large permanent electric dipole moments.

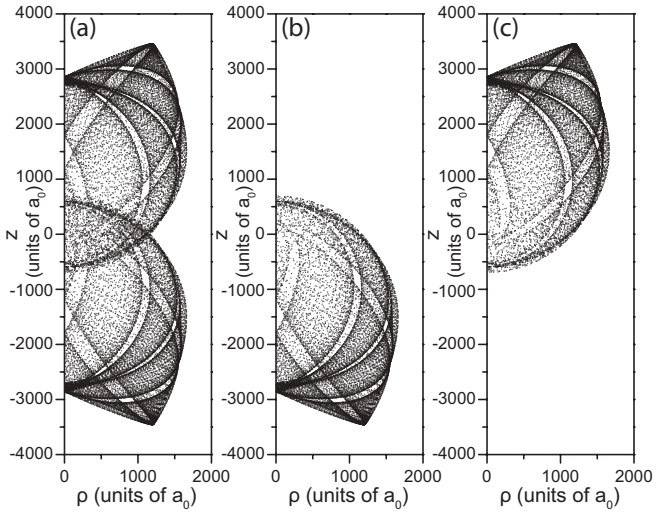

FIG. 9. Classical electron trajectories at an energy of $\sim -55.1\ \mathrm{cm}^{-1}$, $B_{\mathrm{th}} = 2.580$ T. The simulated trajectory duration is 137 ns and the electron position is plotted every 8.2 ps. At $F = 0$, the sum of the point densities of two equivalent trajectories (a) mimics the wave-function probabilities in Fig. 7. At small but nonzero F, the point densities of individual, slightly nondegenerate trajectories (b) and (c) mimic the wave-function probabilities in Fig. 8.

Initial conditions are chosen such that the trajectories mimic the wave-function probabilities in Figs. 7 and 8. Over short time scales, the trajectories are Kepler-like. Over longer times the eccentricity and alignment vary in a periodic fashion. The alignment wobbles about the z direction, which is one of the reasons why the corresponding quantum states have been labeled as "vibrator states." At $F = 0$, the trajectories displayed in Fig. 9(a) are exactly equivalent. The wave-function probabilities of corresponding quantum states must mimic the sum of the point densities of the two equivalent trajectories. Figure 9(a) indeed closely resembles the wave-function probabilities in Fig. 7. If a weak parallel electric field is added, both classical and quantum degeneracies are lifted. In that case, the wave-function probabilities of corresponding quantum states mimic the point density of only one of the two trajectories. This applies to the wave-function probabilities shown in Fig. 8, which closely resemble Figs. 9(b) and 9(c).

VII. DISCUSSION

We have performed high-resolution spectroscopy of rubidium Rydberg atoms in parallel electric and magnetic fields in the n-mixing regime. The spectra contain residual pairs of near-degenerate vibrator states embedded in an otherwise nondegenerate spectrum. Small changes of the B field have been used to tune a sample pair of such states into resonance. An additional weak, parallel electric field has then been applied to prepare states with large electric dipole moments. In the theoretical component of our work, we have reproduced the experimentally observed spectra and analyzed the distribution of states with respect to their electric and magnetic dipole moments and their optical excitation rates. In the following we briefly discuss possible future work.

Dipolar states of Rydberg atoms in strong magnetic and weak parallel electric fields are good candidates for Rydberg-atom interaction studies and applications thereof. They are nondegenerate and have high optical excitation rates from low-lying atomic states. The states we have labeled the X pair have dipole moments of $p_0 \approx 1500\, ea_0$. The electric-dipole interaction energy between two such atoms, $E_{\mathrm{dd}} \sim p_0^2/(4\pi\epsilon_0 d^3)$, amounts to several tens of megahertz at a distance $d = 5\ \mu$m. This level of interaction strength is within the desirable range for applications. For instance, the implementation of a phase gate akin to that in Ref. [10] would require optical excitation pulses of less than about 1 μs in duration, leading to total gate times of a few microseconds. This is fast enough that atomic decay can largely be neglected. As a second example of quantum control, consider a pair of Rydberg atoms in one of the X pair levels at a distance $d = 10\ \mu$m, in a magnetic field where the two states are nondegenerate and separated by an energy defect $\Delta E = h \times 100$ MHz at $F = 0$. A smooth electric field pulse $F(t)$ that begins and ends at zero is applied. The time-dependent electric dipole moment $p(t) = F(t)p_0^2/\sqrt{\Delta E^2/4 + F(t)^2 p_0^2 a^2}$, where $p_0 \approx 1500\, ea_0$, and the acquired interaction-induced phase $|\Delta\phi| \sim \int p^2(t)dt/(4\pi\epsilon_0\hbar d^3)$. To implement a 2π phase shift, an electric field pulse with a peak field of several V/m and a duration of about 1 μs would be needed. This is short compared to the atomic lifetime, but long enough to ensure adiabatic evolution [which requires a ramp duration $t_{\mathrm{ramp}} \gg h/(\Delta E) = 10$ ns].

Magnetic dipole interactions between pairs of diamagnetic Rydberg atoms are in the subhertz range and are negligible. However, the magnetic dipole moments determine the suitability for magnetic trapping. Values in the range $\lesssim -10\mu_B$, as encountered in the X pair of levels, are ideal for that purpose. Although Rydberg-atom trapping has previously been accomplished using optical and electrostatic interactions, magnetic trapping of specific well-defined states is still to be demonstrated. Diamagnetic Rydberg levels in the n-mixing regime are suitable for this purpose due to their combination of high optical excitation rates and large magnetic dipole moments.

Diamagnetic Rydberg atoms can be expected to exhibit many Förster resonances. In a Förster energy-exchange process, two atoms or molecules undergo an energy-conserving state change $|\psi_A\rangle + |\psi_B\rangle \rightarrow |\psi_C\rangle + |\psi_D\rangle$, where states $|\psi_A\rangle$ and $|\psi_C\rangle$ are electric dipole coupled, as are states $|\psi_B\rangle$ and $|\psi_D\rangle$. Förster resonances have been studied widely as a method to generate long-range Rydberg atom interactions (see, for instance, [6,13]). Rydberg atoms in strong magnetic and weak electric fields offer a nondegenerate spectrum at a much higher density of optically accessible states than Rydberg atoms in zero or weak fields. Hence, one may expect to find numerous Förster resonances. Two field parameters B and F would be available to tune their energy defects. Work in this direction is in progress.

ACKNOWLEDGMENTS

This work was supported by the Chemical Sciences, Geosciences and Biosciences Division of the Office of Basic Energy Sciences, Office of Science, US Department of Energy, and NSF Grant No. PHY-0855871. E.P. acknowledges support from the Natural Sciences and Engineering Research Council of Canada.

[1] D. Jaksch, J. I. Cirac, P. Zoller, S. L. Rolston, R. Côté, and M. D. Lukin, Phys. Rev. Lett. **85**, 2208 (2000).
[2] E. Urban, T. A. Johnson, T. Henage, L. Isenhower, D. D. Yavuz, T. G. Walker, and M. Saffman, Nat. Phys. **5**, 110 (2009).
[3] H. Kübler, J. P. Shaffer, T. Baluktsian, R. Löw, and T. Pfau, Nat. Photonics **4**, 112 (2010).
[4] T. Vogt, M. Viteau, J. Zhao, A. Chotia, D. Comparat, and P. Pillet, Phys. Rev. Lett. **97**, 083003 (2006).
[5] T. Vogt, M. Viteau, A. Chotia, J. Zhao, D. Comparat, and P. Pillet, Phys. Rev. Lett. **99**, 073002 (2007).
[6] A. Reinhard, K. C. Younge, and G. Raithel, Phys. Rev. A **78**, 060702 (2008).
[7] D. Tong, S. M. Farooqi, J. Stanojevic, S. Krishnan, Y. P. Zhang, R. Côté, E. E. Eyler, and P. L. Gould, Phys. Rev. Lett. **93**, 063001 (2004).
[8] R. Heidemann, U. Raitzsch, V. Bendkowsky, B. Butscher, R. Löw, L. Santos, and T. Pfau, Phys. Rev. Lett. **99**, 163601 (2007).
[9] T. Wilk, A. Gaëtan, C. Evellin, J. Wolters, Y. Miroshnychenko, P. Grangier, and A. Browaeys, Phys. Rev. Lett. **104**, 010502 (2010).
[10] L. Isenhower, E. Urban, X. L. Zhang, A. T. Gill, T. Henage, T. A. Johnson, T. G. Walker, and M. Saffman, Phys. Rev. Lett. **104**, 010503 (2010).
[11] H. Friedrich, *Theoretical Atomic Physics*, 2nd ed. (Springer-Verlag, Berlin, 1998).
[12] T. F. Gallagher, *Rydberg Atoms* (Cambridge University Press, New York, 1994).
[13] W. R. Anderson, J. R. Veale, and T. F. Gallagher, Phys. Rev. Lett. **80**, 249 (1998).
[14] K. A. Safinya, J. F. Delpech, F. Gounand, W. Sandner, and T. F. Gallagher, Phys. Rev. Lett. **47**, 405 (1981).
[15] P. Bohlouli-Zanjani, J. A. Petrus, and J. D. D. Martin, Phys. Rev. Lett. **98**, 203005 (2007).
[16] T. G. Walker and M. Saffman, J. Phys. B **38**, S309 (2005).
[17] J. C. Gay and D. Delande, Comments At. Mol. Phys. **13**, 275 (1983).
[18] T. van der Veldt, W. Vassen, and W. Hogervorst, J. Phys. B **26**, 1945 (1993).
[19] M. L. Zimmerman, J. C. Castro, and D. Kleppner, Phys. Rev. Lett. **40**, 1083 (1978).
[20] P. Cacciani, E. Luc-Koenig, J. Pinard, C. Thomas, and S. Liberman, Phys. Rev. Lett. **56**, 1124 (1986).
[21] J. R. Guest, J.-H. Choi, E. Hansis, A. P. Povilus, and G. Raithel, Phys. Rev. Lett. **94**, 073003 (2005).
[22] E. Paradis, S. Zigo, K. Z. Hu, and G. Raithel, Phys. Rev. A **86**, 023416 (2012).
[23] J. L. Wiza, Nucl. Instrum. Methods **162**, 587 (1979).
[24] M. C. Gutzwiller, *Chaos in Classical and Quantum Mechanics* (Springer, New York, 1990).
[25] Replace $(n_1 - n_2)$ by $(n - 1)$ in Eq. 6.14 of T. F. Gallagher, *Rydberg Atoms* [12].
[26] J. Han, Y. Jamil, D. V. L. Norum, P. J. Tanner, and T. F. Gallagher, Phys. Rev. A **74**, 054502 (2006).